Available online at www.sciencedirect.com

ScienceDirect

Comput. Methods Appl. Mech. Engrg. 275 (2014) 98–112

Computer methods in applied mechanics and engineering

www.elsevier.com/locate/cma

Detection of multiple flaws in piezoelectric structures using XFEM and level sets

S.S. Nanthakumar [a], T. Lahmer [a], T. Rabczuk [a,b,*]

[a] Institute of Structural Mechanics, Bauhaus-University Weimar, Marienstr. 15, D-99423 Weimar, Germany
[b] School of Civil, Environmental and Architectural Engineering, Korea University, Seoul, Republic of Korea

Received 30 November 2013; received in revised form 15 February 2014; accepted 1 March 2014
Available online 19 March 2014

Abstract

An iterative procedure to solve the inverse problem of detecting multiple voids in piezoelectric structure is proposed. In each iteration the forward problem is solved for various void configurations, and at each iteration, the mechanical and electrical responses of a piezoelectric structure is minimized at known specific points along the boundary to match the measured data. The Extended Finite Element method (XFEM) is employed for determining the responses as it allows the use of a fixed mesh for varying void geometries. The numerical method based on combination of classical shape derivative and of the level-set method for front propagation used in structural optimization is utilized to minimize the cost function. The results obtained show that this method is effectively able to determine the number of voids in a piezoelectric structure and its corresponding locations and shapes.

Keywords: Inverse problem; XFEM; Level set method; Piezoelectric ceramics

1. Introduction

Piezoelectric materials deform when subjected to an electric field and produce an electric field when stressed. This intrinsic coupling behavior of piezoelectric materials has attracted wide applications in electro-mechanical and electronic devices such as electro-mechanical actuators, sensors and transducers. In general, some defects like voids or cracks may be produced in piezoelectric materials during the manufacturing process. When they are subjected to mechanical and electrical loads, stress concentrations due to these defects may lead to critical crack growth and subsequent mechanical failure or dielectric breakdown. Many researchers have studied the

* Corresponding author at: Institute of Structural Mechanics, Bauhaus-University Weimar, Marienstr. 15, D-99423 Weimar, Germany. Tel.: +49 15211501784.
E-mail addresses: nanthakumar.srivilliputtur.subbiah@uni-weimar.de (S.S. Nanthakumar), tom.lahmer@uni-weimar.de (T. Lahmer), timon.rabczuk@uni-weimar.de (T. Rabczuk).

http://dx.doi.org/10.1016/j.cma.2014.03.001
0045-7825/

behavior of these materials in the presence of defects; fundamentals of piezoelectric fracture mechanics can be found in [1–4]. A short overview and a critical discussion about the present state in the field of piezoelectric fracture mechanics is given in [5]. Application of piezoelectric fracture mechanics to realistic crack configurations and loading situations requires an effective numerical method like the Finite Element Method (FEM), meshfree methods, phantom node or numerical manifold method [6] or DDA [7]. A review on the state of art of applying FEM to analyse cracks in 2D and 3D piezoelectric structures is given in [8].

In Rus et al. [9] a series of studies on damage detection in piezoelectric materials is presented, in which the inverse problem is solved iteratively using the FEM and Boundary Element Method (BEM). In this work, the cost functional is minimized using a Genetic Algorithm (GA). An enhanced iterative scheme for the precise reconstruction of piezoelectric material parameters from electric impedance and mechanical displacement measurement is presented in [10]. In works related to crack or void identification a remeshing of the finite element domain is required in each iteration of the optimization scheme to solve the inverse problem. Mesh free methods [11–16] do not require remeshing and they have been used to solve inverse problems [17] iteratively. On the other hand, the Extended Finite Element method (XFEM) has been utilized to solve the forward problem in each iteration in [18,19]. In XFEM [20,21], the displacement field is enriched near the crack face by incorporating both discontinuous fields and near tip asymptotic fields through a partition of unity method. XFEM exploits the partition of unity property of Finite Elements identified by Melenk and Babuska [22], which allows local enrichment functions to be easily incorporated into a Finite Element approximation. In XFEM, implicit level set functions are used to model cracks [23], holes and material interfaces (inclusions) [24]. Some improvements in XFEM are proposed in [25] so as to obtain improved performances. Application of XFEM to the analysis of fracture in piezoelectric materials is presented in Bechet et al. [26], where new crack tip enrichment functions suitable for cracks in piezoelectric structures are proposed. An Extended Finite Element formulation for dynamic fracture of piezoelectric materials is developed in [27]. The inverse problem of detecting cracks and voids in 2D piezoelectric structures using XFEM is presented in [28]. The optimization schemes utilized commonly in solving the inverse problem of damage detection are Genetic Algorithm [18] and global search methods [28]. The number of iterations in these methods increases in proportion to the number of parameters used to define the flaws. Because of this limitation, most previous studies were restricted to detecting only one single void or crack of simple geometry. For example, in [28], the void is explicitly defined using five parameters. These parameters are determined such that the objective function is minimized using Multilevel Coordinate Search [29] as the optimization algorithm. The algorithm proposed can determine the location and equivalent elliptical shape of only one single void in a piezoelectric structure.

A new numerical method based on the combination of the classical shape derivative and of the level-set method for front propagation in the context of structural optimization is proposed in [30]. XFEM based level set schemes for structural optimization are presented in [31].

The aim of this paper is to propose a strategy to detect multiple voids in 2D piezoelectric structures by combining shape derivative and level sets as employed in structural optimization problems. XFEM, in addition to independence of background mesh to flaw configuration, utilizes implicit level set functions for defining flaws. Thereby, it becomes a natural choice for solving the forward problem in each iteration for different flaw configurations.

The outline of the paper is as follows. Sections 2 and 3 are about piezoelectric governing equations and the piezoelectric Extended Finite Elements formulation respectively. Section 4 comprises details on combining shape derivative and level set method to minimize the objective function and thereby detecting the location of voids. Section 5 shows numerical examples to prove the ability of this method in solving the intended inverse problem iteratively.

2. Basic piezoelectric relations

The constitutive equations of a linear piezoelectric material are,

$$\sigma_{ij} = C^{E}_{ijkl}\varepsilon_{kl} - e_{kij}E_k, \tag{1}$$

$$D_i = e_{ikl}\varepsilon_{kl} + \kappa^{\varepsilon}_{ik}E_k. \tag{2}$$

In (1) and (2), C^E_{ijkl}, e_{kij} and $\kappa^{\varepsilon}_{ik}$ denote the elastic stiffness at constant electric field E, the piezoelectric constant and dielectric permittivity at constant strain ε, respectively. These tensors are experimentally determined for various piezoelectric materials or by model fitting strategies. The mechanical strain tensor is determined by the gradient of the mechanical displacement and the electric field is found by differentiation of the electric potential as follows

$$\varepsilon_{ij} = \frac{1}{2}\left(\left(u_{i,j}\right) + \left(u_{j,i}\right)\right), \tag{3}$$

$$E_i = -\phi^e_{,i}. \tag{4}$$

The basic laws governing the behavior of piezoelectric materials in domain Ω with boundary Γ $(= \Gamma_e \cup \Gamma n)$ are the balance equations of mechanical momentum and electric charges

$$\sigma_{ij,j} + f_i = 0 \text{ in } \Omega, \tag{5}$$

$$D_{i,i} - q = 0 \text{ in } \Omega. \tag{6}$$

In the above equations, f_i and q are mechanical body force components and electric body charge, respectively; σ_{ij} and D_i are the Cauchy stress tensor and the electric displacement vector components respectively. The essential and natural boundary conditions, to which the piezoelectric material is subjected to are Essential boundary conditions

$$u = \bar{u} \text{ (or) } ; \phi^e = \bar{\phi}^e \text{ on } \Gamma_e. \tag{7}$$

Natural boundary conditions

$$\sigma_{ij} n_j = F_i \text{ (or) } D_i n_i = -Q \text{ on } \Gamma_n, \tag{8}$$

where $\bar{u}$, $\bar{\phi}$, F_i, Q and n_i are mechanical displacement, electric potential, surface force components, surface charge and outward unit normal vector components respectively. The void boundary V is assumed traction free while limited permeability boundary condition is assumed in crack faces C^+ and C^-, i.e., the crack faces are subjected to electrical traction, the magnitude of which depends on the crack opening displacement (see Fig. 1).

3. Extended Finite Element formulation

The XFEM displacement, u^h and electric potential, ϕ^{e^h} fields for a piezoelectric material are given as,

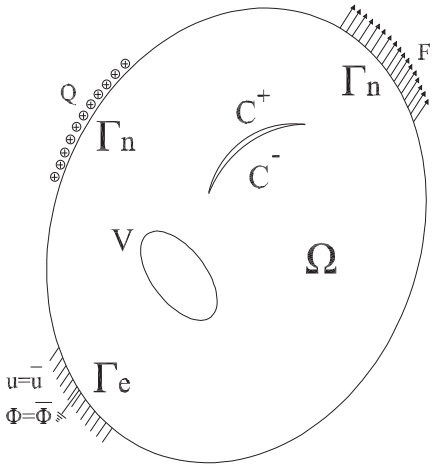

Fig. 1. Piezoelectric domain with a crack.

$$u^h(x) = \sum_{i\in I} N_i(X)u_i + \sum_{N=1}^{n_c}\sum_{j\in J} N_j(X)a_j^{(N)}\psi_I^{(N)} + \sum_{M=1}^{m_t}\sum_{k\in K} N_k(X)\left(\sum_{i=1}^{4}\Phi_i^{(M)}(r,\theta)b_k^i\right), \tag{9}$$

$$\phi^{e^h}(x) = \sum_{i\in I} N_i(X)\phi_i + \sum_{N=1}^{n_c}\sum_{j\in J} N_j(X)\alpha_j^{(N)}\psi_I^{(N)} + \sum_{M=1}^{m_t}\sum_{k\in K} N_k(X)\left(\sum_{i=1}^{4}\Phi_i^{(M)}(r,\theta)\beta_k^i\right), \tag{10}$$

where n_c denotes the number of cracks/voids, m_t is the number of crack tips, and l is the number of additional degrees of freedom of crack tip enriched nodes; J is the set of all nodes whose support is cut by crack face or void boundary while set K contains all the nodes that lie within a fixed area around the crack tips [32], a_j, b_k are the additional degrees of freedom to be found along with nodal displacements while α_j, β_k are the additional degrees of freedom to be found along with nodal electric potentials.

The cracks and voids are implicitly represented by level set functions in XFEM [23,24]. The level set function for modeling void boundary is a signed distance function, with negative and positive values on either side of the boundary. In order to represent cracks two level set functions i.e. normal, ψ and tangential, ϕ level set functions, are required. The crack tips are therefore given by the intersection of these level set functions. The crack face is represented by the zero normal level set function having negative ϕ values.

In case of voids, the value of $\psi^{(N)}$ in Eqs. (9) and (10) are 0 and 1 inside and outside the voids, respectively. The nodes that lie exactly on the void boundary are considered as FEM nodes and are not enriched [24]. The terms corresponding to the second enrichment function will not be required in Eqs. (9) and (10). In case of cracks, the shifted step function is used to represent the jump in the displacement and electric potential fields for those nodes that lie in set J. Bechet et al. [26] proposed special enrichment functions to represent the field behavior in the vicinity of the crack tip in piezoelectric materials. He also concluded that the results obtained using the enrichment functions used in isotropic elasticity are as good as that obtained by using specific six fold enrichment functions for electro mechanical fracture modeling.

Substituting the Extended Finite Elements approximation (9) and (10) into the weak form finally yields the discrete form of the equilibrium equations,

$$\left[K^{UU}\right]\begin{Bmatrix} u \\ a \\ b \end{Bmatrix} + \left[K^{U\Phi}\right]\begin{Bmatrix} \phi^e \\ \alpha \\ \beta \end{Bmatrix} = \begin{Bmatrix} f_u \\ f_u^a \\ f_u^b \end{Bmatrix}, \tag{11}$$

$$\left[K^{\Phi U}\right]\begin{Bmatrix} u \\ a \\ b \end{Bmatrix} - \left[K^{\Phi\Phi}\right]\begin{Bmatrix} \phi^e \\ \alpha \\ \beta \end{Bmatrix} = \begin{Bmatrix} f_\phi \\ f_\phi^\alpha \\ f_\phi^\beta \end{Bmatrix}, \tag{12}$$

$$K^{UU} = \begin{pmatrix} \int_\Omega B_{ui}^T C B_{uj} d\Omega & \int_\Omega B_{ui}^T C B_{uj}\psi_j^{(N)} d\Omega & \int_\Omega B_{ui}^T C B_{uj}\Phi_j^{(M)} d\Omega \\ \int_\Omega B_{uj}^T C B_{ui}\psi_i^{(N)} d\Omega & \int_\Omega \psi_i^{(N)} B_{ui}^T C B_{uj}\psi_j^{(N)} d\Omega & \int_\Omega \psi_i^{(N)} B_{ui}^T C B_{uj}\Phi_j^{(M)} d\Omega \\ \int_\Omega B_{uj}^T C B_{ui}\Phi_i^{(M)} d\Omega & \int_\Omega \psi_j^{(N)} B_{uj}^T C B_{ui}\Phi_i^{(M)} d\Omega & \int_\Omega \Phi_i^{(M)} B_{ui}^T C B_{uj}\Phi_j^{(M)} d\Omega \end{pmatrix},$$

$$K^{U\Phi} = \begin{pmatrix} \int_\Omega B_{ui}^T e B_{\phi j} d\Omega & \int_\Omega B_{ui}^T e B_{\phi j}\psi_j^{(N)} d\Omega & \int_\Omega B_{ui}^T e B_{\phi j}\Phi_j^{(M)} d\Omega \\ \int_\Omega \psi_j^{(N)} B_{uj}^T e B_{\phi i} d\Omega & \int_\Omega \psi_i^{(N)} B_{ui}^T C B_{uj}\psi_j^{(N)} d\Omega & \int_\Omega \psi_i^{(N)} B_{ui}^T e B_{\phi j}\Phi_j^{(M)} d\Omega \\ \int_\Omega \Phi_j^{(M)} B_{uj}^T e B_{\phi i} d\Omega & \int_\Omega \Phi_j^{(M)} B_{uj}^T e B_{\phi i}\psi_i^{(N)} d\Omega & \int_\Omega \Phi_i^{(M)} B_{ui}^T e B_{\phi j}\Phi_j^{(M)} d\Omega \end{pmatrix},$$

$$K^{\Phi U} = \left(K^{U\Phi}\right)^T;$$

$$K^{\Phi\Phi} = \begin{pmatrix} \int_\Omega B_{\phi i}^T \kappa B_{\phi j} d\Omega & \int_\Omega B_{\phi i}^T \kappa B_{\phi j}\psi_j^{(N)} d\Omega & \int_\Omega B_{\phi i}^T \kappa B_{\phi j}\Phi_j^{(M)} d\Omega \\ \int_\Omega B_{\phi j}^T \kappa B_{\phi i}\psi_i^{(N)} d\Omega & \int_\Omega \psi_i^{(N)} B_{\phi i}^T \kappa B_{\phi j}\psi_j^{(N)} d\Omega & \int_\Omega \psi_i^{(N)} B_{\phi i}^T \kappa B_{\phi j}\Phi_j^{(M)} d\Omega \\ \int_\Omega B_{\phi j}^T \kappa B_{\phi i}\Phi_i^{(M)} d\Omega & \int_\Omega \psi_j^{(N)} B_{\phi j}^T \kappa B_{\phi i}\Phi_i^{(M)} d\Omega & \int_\Omega \Phi_i^{(M)} B_{\phi i}^T \kappa B_{\phi j}\Phi_j^{(M)} d\Omega \end{pmatrix}.$$

In the above equations C, e and κ correspond to stiffness, piezoelectric coupling and dielectric permittivity tensors respectively. Numerical integration to determine these stiffness coefficients is performed over sub triangles on either side of the crack face or void boundary. Polar integration approach proposed in [25] is followed for determining stiffness coefficients corresponding to crack tip elements.

4. Inverse problem

The size and location of voids are to be determined, described implicitly by the parameter, P by using measurements on the boundary of the piezoelectric structure which is subjected to mechanical loads.

The displacement and electric potential are the measurements made along the boundary. The forward operator which maps the parameters defining the flaw to measurements on the boundary of the structure is,

$$F : X \rightarrow Y, \tag{13}$$

$$p \mapsto (u, v, \phi^e)_{|\Gamma}. \tag{14}$$

In (13), X denotes the parameter space, i.e. the space of all possible void forms and Y, the space of measurements (displacements and electric potential). ψ^{EXP} contains measurements with noise, the inverse problem corresponds to solving for p in

$$F(p) = \psi^{EXP}, \tag{15}$$

which is approximated by minimizing the least-squares cost functional,

$$J(p) = \left(\sum_{i=1}^{N_{meas}} \left| \psi_i^{EXP} - \psi_i^{XFEM}(p) \right|^2 \right)^{\frac{1}{2}}. \tag{16}$$

In this work the inverse problem of damage detection is solved iteratively. It is obvious that iterative methods are expensive and time consuming because the direct problem has to be solved at each step. XFEM offers the advantage of maintaining a fixed mesh in each iteration while in classical FEM the domain has to be remeshed after each iteration. Therefore in XFEM only the stiffness coefficients corresponding to enriched DOFS vary in each iteration whereas the classical FEM portions of global stiffness matrix, which comprises the bulk of matrix, do not change. Meshing, building nodal connectivity and constructing the entire global stiffness matrix are all surpassed by using XFEM to solve the direct problem in each iteration.

4.1. Shape derivative and level set method

The shape, size and location of voids can be implicitly represented using level sets as shown in Fig. 2. In the process, the location of voids will be identified by change in level set function values, with respect to fictitious

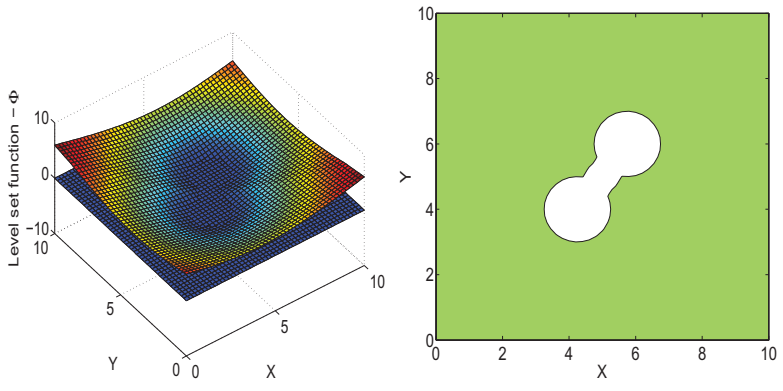

Fig. 2. (a) Contour plot of level set function and (b) the corresponding irregular void boundary.

time, t. The evolution of void shapes, which corresponds to the change in these implicit function, $\phi(x(t)) = 0$ with respect to time, is governed by the Hamilton–Jacobi equation [33],

$$\frac{\partial \phi(x,t)}{\partial t} + V|\nabla \phi| = 0. \tag{17}$$

Moving the level-set isolines along the descent gradient direction is equivalent to transporting ϕ by solving the Hamilton–Jacobi equation. This Hamilton–Jacobi equation is posed not only on the void boundaries but on the entire domain, as the velocity, V is known everywhere. The velocity, V is related to the sensitivity of the objective function to a variation in the level set function values. The change in the objective function due to perturbation of flaw boundaries is given by the shape derivative. The shape derivative is obtained by solving an adjoint problem. In the adjoint case the governing PDEs (5) and (6) are solved with Neumann boundary condition as,

$$\sigma_{ij} n_j = u_i - u_i^{meas} \text{ (and) } D_i n_i = \phi_i^e - \phi_i^{e^{meas}} \text{ on } \Gamma_n \tag{18}$$

and Dirichlet boundary conditions as shown in Eq. (7). The velocity at iteration n in location of node i, V_i^n is given by the shape derivative as shown below,

$$-V_i^n = (grad_\psi J)_i = \sigma_{ij}^p \varepsilon_{ij}^u - D_i^p E_i^u. \tag{19}$$

The subscripts u and p corresponds to actual and adjoint state respectively. The Hamilton–Jacobi equation is posed not only on the void boundary but in the entire domain, as the velocity, V can be computed everywhere. Hamilton–Jacobi equations do not usually admit smooth solutions. Existence and uniqueness are obtained in the framework of viscosity solutions which helps in convenient definition of a generalized shape motion. The discrete solution of HJ equation is obtained by an explicit first order upwind scheme [30].

$$\frac{\phi_i^{n+1} - \phi_i^n}{\Delta t} + \min\left(V_i^n, 0\right) g^-\left(D_x^+ \phi_i^n, D_x^- \phi_i^n\right) + \max\left(V_i^n, 0\right) g^+\left(D_x^+ \phi_i^n, D_x^- \phi_i^n\right) = 0 \tag{20}$$

in which,

$$D_x^+ \phi_i^n = \frac{\phi_{i+1}{}^n - \phi_i^n}{\Delta x}, \quad D_x^- \phi_i^n = \frac{\phi_i{}^n - \phi_{i-1}^n}{\Delta x}$$

$$g^+(d^+, d^-) = \sqrt{\min(d^+, 0)^2 + \max(d^-, 0)^2},$$

$$g^-(d^+, d^-) = \sqrt{\max(d^+, 0)^2 + \min(d^-, 0)^2}.$$

The level set function is periodically regularized by solving,

$$\frac{\partial \phi}{\partial t} + sign(\phi_0)(|\nabla \phi| - 1) = 0. \tag{21}$$

The solution to this equation is a signed distance function to an initial isoline, ϕ_0. Extended finite element analysis performed in each iteration requires a signed distance value from crack or inclusion boundary in order to determine enrichment function values and so the regularization step is performed in each iteration.

The steps involved in this void detection algorithm are as follows,

- Initialization of level set function ϕ_0 is done. In order to avoid local optima the voids are uniformly distributed all over the domain.
- Computation of actual state u_k and adjoint state p_k is performed. These are determined by solving Eqs. (5) and (6) posed in domain Ω_k with essential boundary condition shown in Eq. (7) and two different natural boundary conditions shown in Eqs. (8) and (19) for actual and adjoint states respectively. Using Eq. (19), the velocity to move the void boundary (i.e.) the shape derivative is determined.
- The new void configuration is given by the level-set function ϕ_{k+1} by solving the transport Hamilton–Jacobi equation (17) after a fictitious time step Δt_k starting from the initial shape ϕ_k with velocity v_k computed in terms of u_k and p_k.

- The level set values are regularized by solving Eq. (21) as ϕ_{k+1} is no more a signed distance function.
- The algorithm is stopped when there is no significant reduction in objective function, (i.e.) when the gradient of objective function is less than a fixed tolerance value, which can also be seen from no significant change in void configuration with iterations.

5. Numerical examples

The effectiveness of the combination of the XFEM and the proposed level set based optimization algorithm is tested by several flaw detection problems. In the examples, a plate (10×10 units) made of PZT-5H with material properties shown in Table 1 is considered. Plane strain assumption is used. The material properties are such that the piezoelectric plate is poled in y direction as shown in Fig. 3. The elastic constants, the dielectric permittivity constants and the piezoelectric constants are of different orders, so the stiffness matrix might be ill-conditioned and lead to unstable results. Hence in order to improve the condition number of the stiffness matrix we make use of the dimension changing method described in [34,35].

As shown in Fig. 3, the piezoelectric plate is subjected to a mechanical line load (T_{yy}) at edge 3 while edge 1 is fixed; the electric potential is set to zero. The horizontal displacement, u, the vertical displacement, v and the electric potential ϕ are measured along the edge 2 of the plate at 25 uniformly spaced sensor locations. In Rus et al.[9], a similar setup is employed to detect voids in a piezoelectric plate and it was shown that the excitation of the piezoelectric specimen by a static mechanical traction transverse to the polarization direction provides better identifiability than applying a static electrical load. The response data from four sets of experiments are utilised in each iteration. When edge 1 is fixed, T_{yy} is applied at edge 3. When edge 2 is fixed, T_{yy} is applied at edge 4 and so on. More than one setup is required to serve two purposes. First, to overcome the problem of

Table 1
Properties of piezoelectric material.

Elastic constants	Piezoelectric constants	Dielectric constants
$C_{11} = 126$ GPa	$e_{21} = -6.5$ C/m^2	$\kappa_{11} = 15.04$ C/(GVm)
$C_{12} = 84.1$ GPa	$e_{22} = 23.3$ C/m^2	$\kappa_{22} = 13$ C/(GVm)
$C_{22} = 117$ GPa	$e_{16} = 17$ C/m^2	
$C_{66} = 23$ GPa		

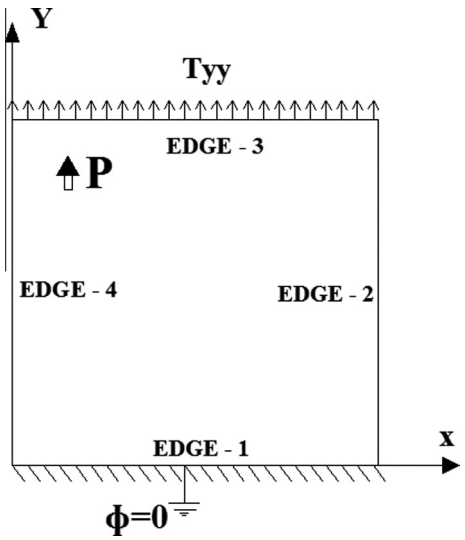

Fig. 3. Boundary conditions and loads on the modeled piezoelectric plate.

converging to local minima and second, when there are two voids exactly one above other, one void might hide the other making it difficult for a single experimental setup to detect their exact locations. Inverse problems are generally ill-posed. Performing several experiments constrains the search space, thereby reducing the ill-posedness and making this problem well-posed.

Measurements

As there are no experimental measurements available for this study, they are simulated numerically by XFEM. Two different mesh sizes are adopted for creating the data and for solving the forward problem so as to avoid "inverse-crimes". In order to generate the target data, a finer mesh compared to the one used for solving the inverse problem is used. Besides, a random noise of about $\pm 1\%$ is added to the generated synthetic data $\psi^{EXP} = \psi^{XFEM}(1 + 0.01\beta)$, where β is a random number between -1 and $+1$.

5.1. Single void

In this example, the location of a single square void is detected using the proposed methodology. The initial assumption is such that the voids are uniformly distributed all over the domain. As it is evident from Fig. 4 with each iteration the trial voids which are distant from the actual void location vanish. The trial voids closer

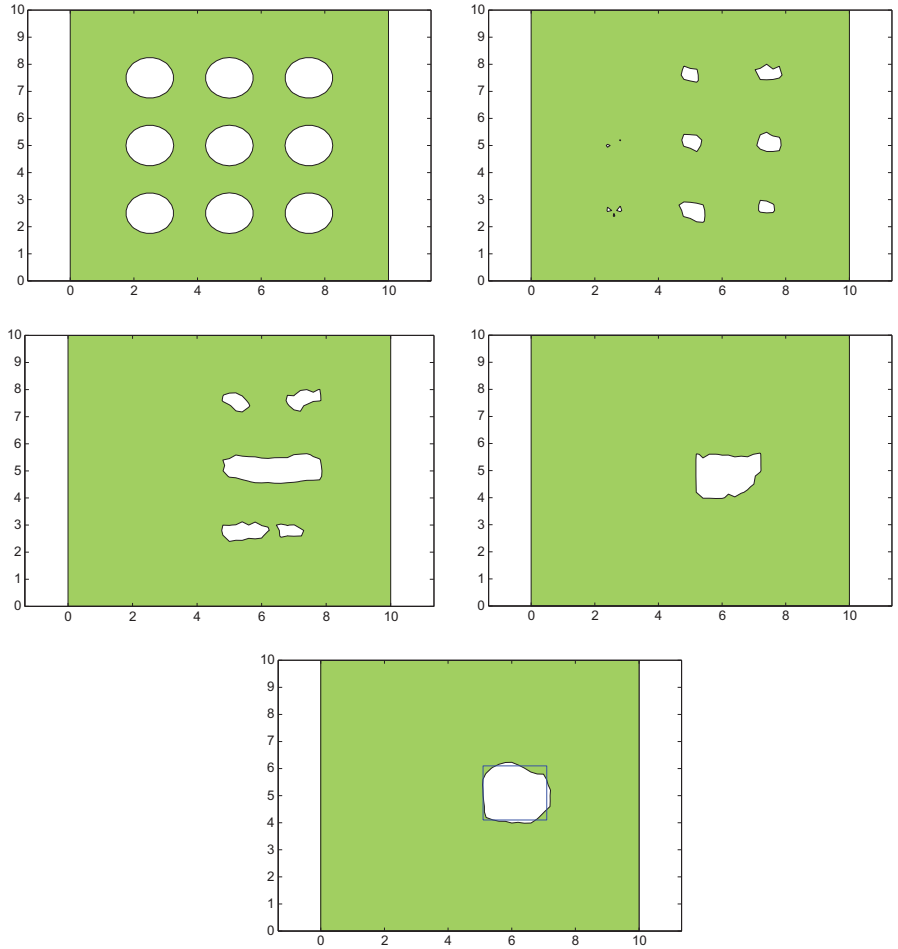

Fig. 4. Top row: initial void configuration, void configuration after 20 iterations, second row: void configuration after 40 and 80 iterations, bottom row: final void configuration and true void.

to the actual void gradually merge together and approach the square shape. This example shows the flexibility of the level set representation of voids which enables their detection of any shape. The explicit representation of void shapes may lead an increased number of parameters corresponding to the least objective function value. Evolutionary or search algorithm may require a higher number of iterations as the number of iterations depend on the number of parameters to be determined. In [28], maximum of 5 parameters defining void shape have been determined with the number of iterations given by $50n^2$, n is the number of parameters, using MCS [29] for optimization. MCS is a zero order method which does not require gradient information. In the current proposed method, the number of iterations is considerably reduced because the gradient information is indirectly obtained from the solution of the adjoint problem. In each iteration, the governing equation is solved twice, once to determine the actual response and then to compute the adjoint variables. The Hamilton–Jacobi equation is solved explicitly, hence the time step is restricted such that it satisfies the CFL condition. Fig. 5 shows the convergence in the spaces Y and X.

5.2. Multiple voids

In this example, the location and the number of several voids present in a piezoelectric structure is detected using the proposed methodology. Similar to the previous example the initial assumption is such that the voids are uniformly distributed all over the domain. As shown in Fig. 6, the trial voids far from the actual voids gradually reduce in size and finally vanish. The trial voids lying within or along the boundary of the actual voids merge and change shape until they match the shape of actual voids. This example shows that the number of iterations is almost independent of the number of voids to be determined. The level set function is updated in each iteration by solving the HJ equation explicitly. The number of explicit time steps required to solve the HJ equation varies. For each XFEM analysis, 10 explicit time steps of the HJ transport equation is performed. Depending on the reduction in the objective function values, this number is gradually reduced such that the objective function values decreases with increasing number of iterations. Solving this inverse problem of multiple voids using search algorithm requires explicitly parametrizing the multiple void locations and their shapes. The number of parameters cannot be known a priori as the number of voids in the piezoelectric plate is unknown. This proposed method is able to determine, how many number of voids are present in the structure and where they are located. The algorithm predicts three voids in the structure and their corresponding locations. Fig. 7 shows the convergence of the algorithm.

5.3. Cracks

In this example, the approximate location of cracks is detected using voids uniformly distributed over the domain as initial assumption. The algorithm is expected to determine the equivalent elliptical void location in the structure whose boundary measurements match with that of the cracked piezoelectric structure. The target data is generated by solving the piezoelectric structure with cracks by XFEM and the resulting boundary displacement and electrical potential values are added with noise. As stated earlier, semi-permeable boundary

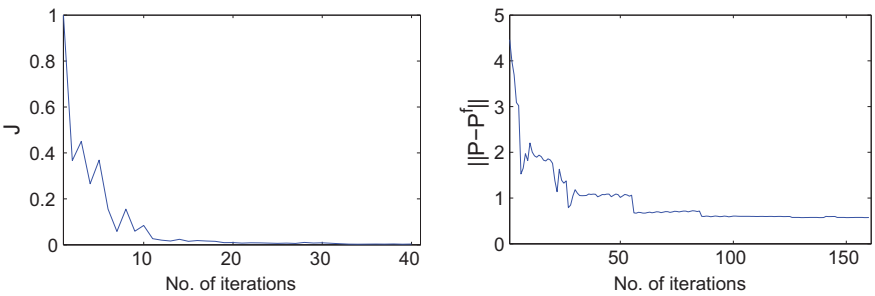

Fig. 5. (a) Convergence of the objective function, J with iteration and (b) convergence of L^2 norm of error in parameter space with iterations. P, approximated level set value at nodes and P^f, level set values corresponding to true void configuration.

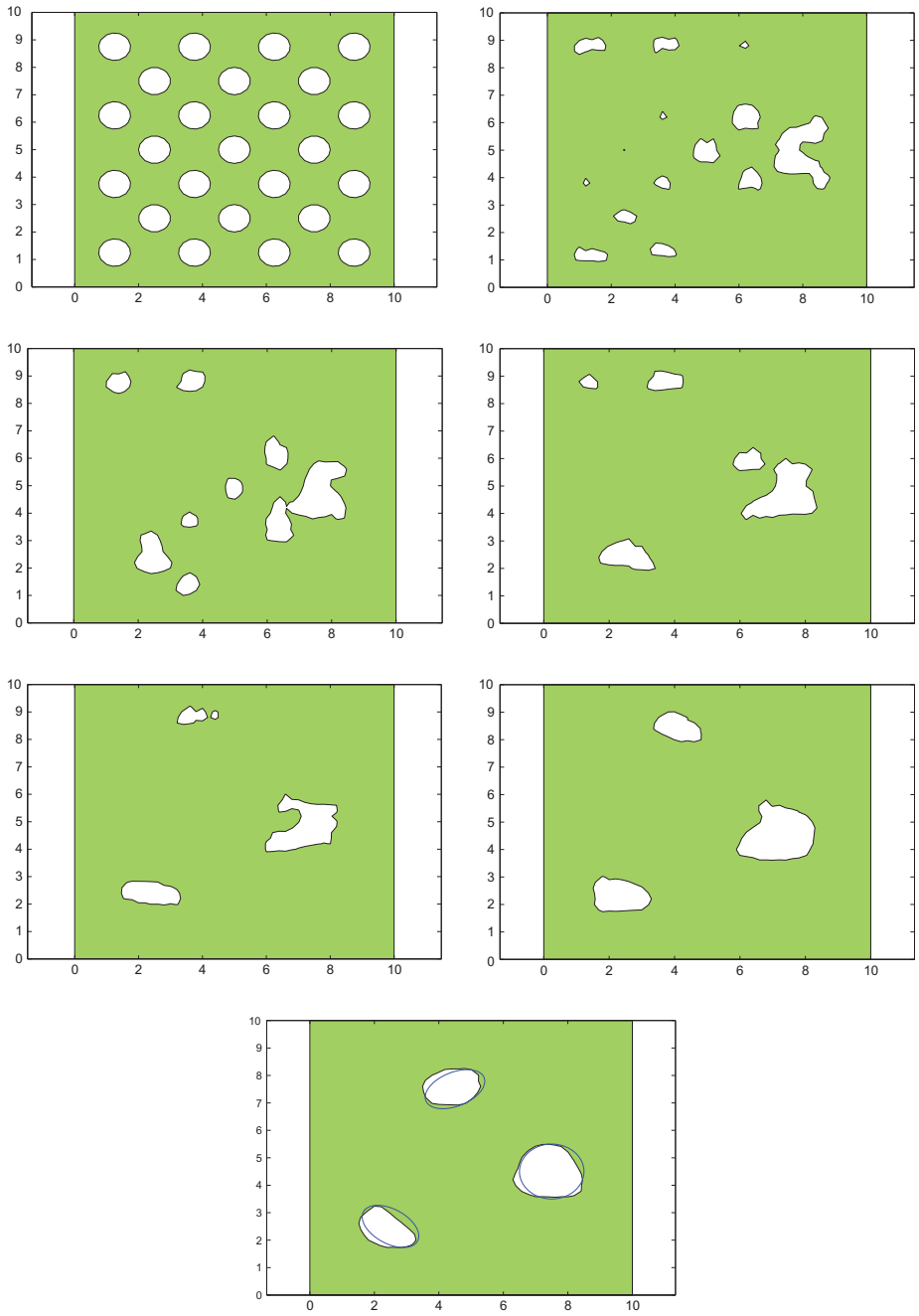

Fig. 6. Top row: initial void configuration, void configuration after 20 iterations, second row: void configuration after 30 and 50 iterations, bottom row: void configuration after 100 and 150 iterations, final void configuration and true voids.

condition is assumed in the crack face. The iterative capacitor analogy (ICA) proposed by Kuna [8,36] and Hao and Shen [36] is adopted. The electrical displacement along the crack faces depend on electrical potential difference between the crack faces and local crack opening displacement. The surface charges are updated iteratively using Newton algorithm until convergence is achieved. The mechanical displacement and electrical potential values obtained at specific locations along the boundary by analysing piezoelectric structure with semi-permeable cracks is given as target data for the inverse problem.

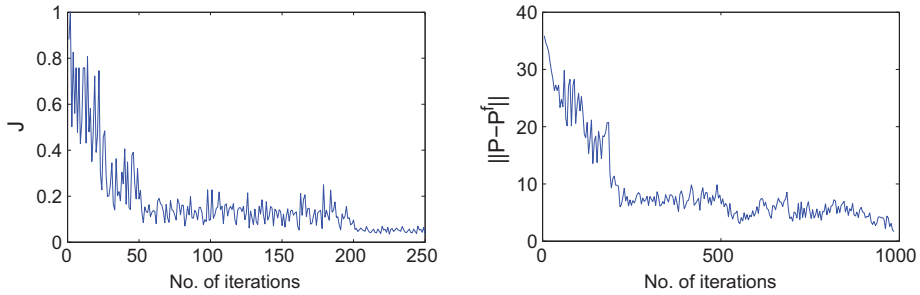

Fig. 7. (a) Convergence of the objective function J over the number of iterations and (b) convergence of l^2 error norm in parameter space over the number of iterations. The approximated level set values are denoted with P and the level set values corresponding to true void configuration with P^f.

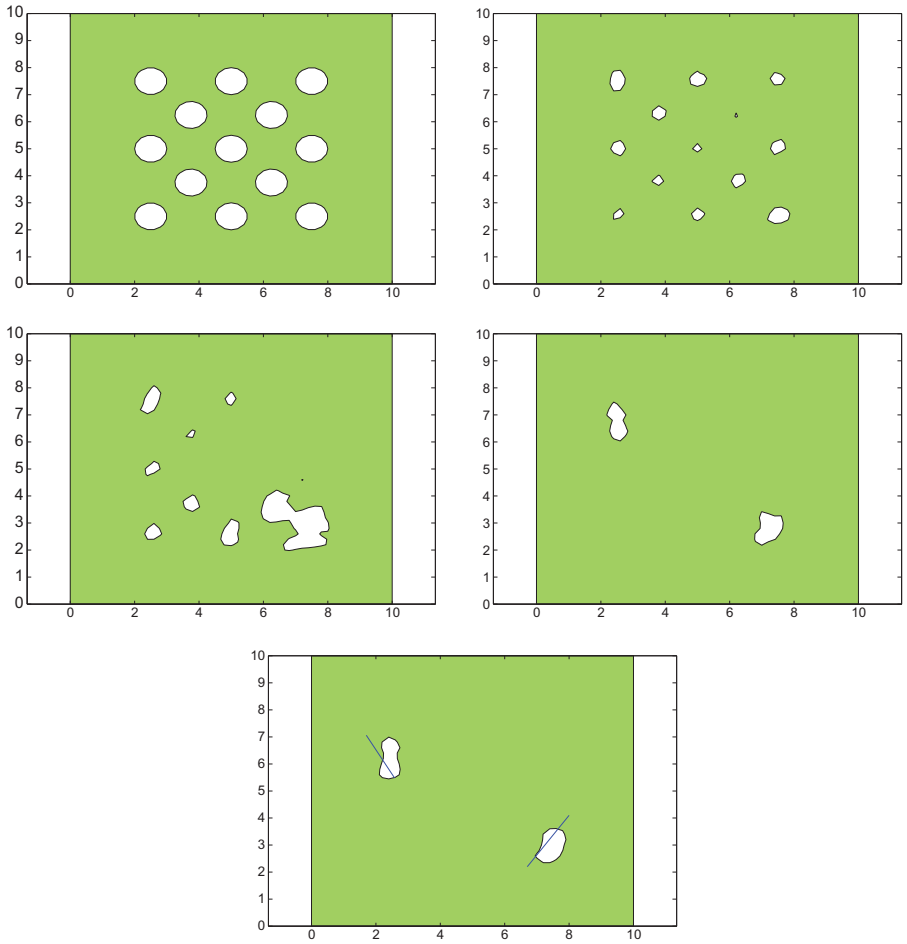

Fig. 8. Top row: initial void configuration, void configuration after 20 iterations, second row: void configuration after 50 and 100 iterations, bottom row: final void configuration and true cracks.

The inverse problem is to determine the location of equivalent elliptical voids which better represent the actual cracks in the structure. Similar to previous examples, the optimization is initiated with voids distributed uniformly all over the domain. The results obtained with increase in iteration is shown in Fig. 8. The piezoelectric domain has two cracks and location of the cracks is detected by the algorithm. The algorithm gives

voids of almost elliptical shape as output in the crack locations. Fig. 9 shows the convergence of the algorithm with iterations. In this example, approximate crack locations are determined using level set representation of voids, which proves that the proposed reconstruction method satisfies the requirement of not committing an inverse crime.

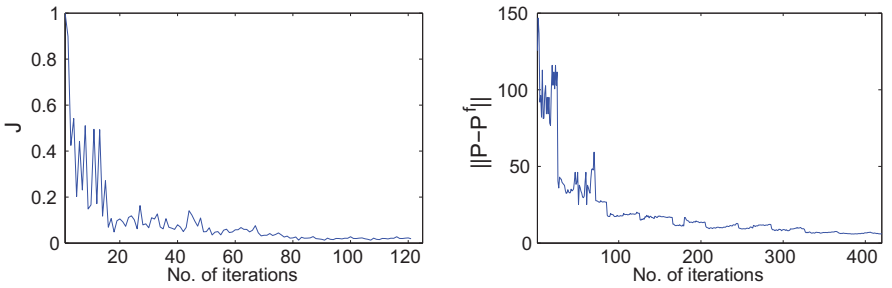

Fig. 9. (a) Convergence of the objective function J over the number of iterations and (b) convergence of l^2 error norm in parameter space over the number of iterations. The approximated level set values are denoted with P and with P^f the level set values corresponding to true void configuration.

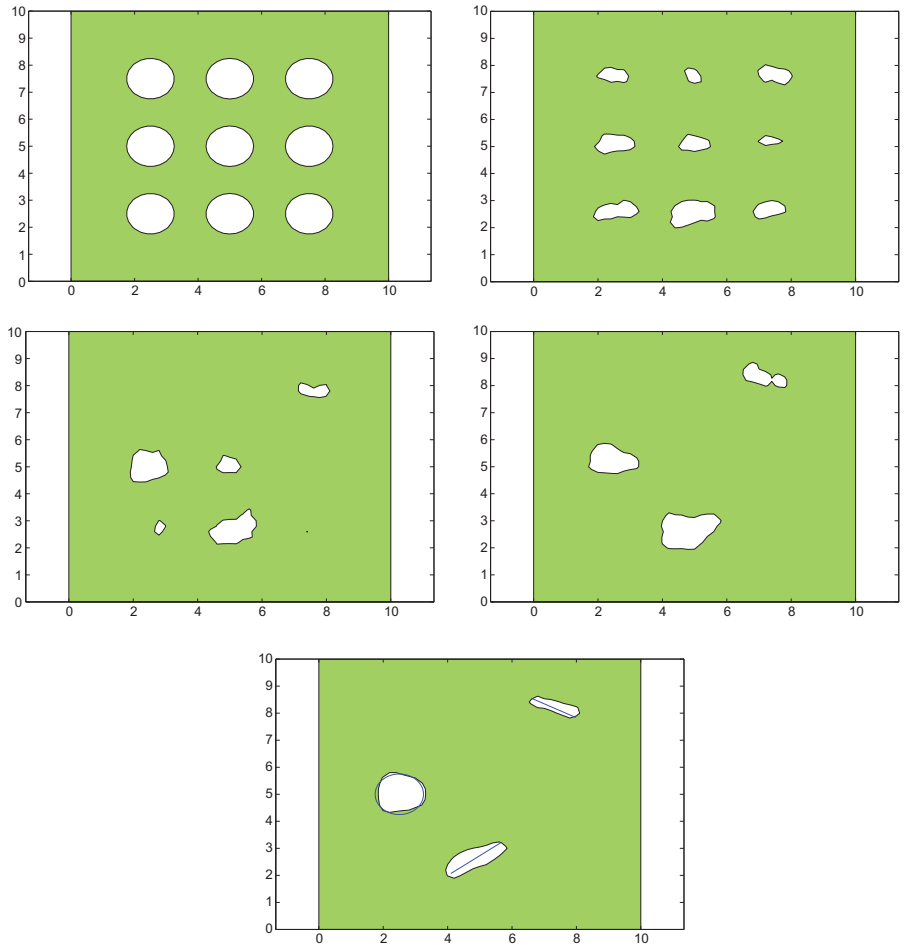

Fig. 10. Top row: initial void configuration, void configuration after 20 iterations, second row: void configuration after 50 and 100 iterations, bottom row: final void configuration and true void/ cracks.

5.4. Voids and cracks

In this example, a more general damaged domain is studied. The structure contains both cracks and voids which is common in an actual piezoelectric domain. The algorithm should be able to locate the defects. Initially voids are assumed to be located all over the domain. As the iteration progresses, the voids that are located near a crack or void remains while other voids disappear. The remaining voids, gradually change shape into an almost elliptical void at the crack location. They also tend to the actual void profile at the void location. Fig. 10 shows that the algorithm is able to detect the location of all three defects. Fig. 11 shows the convergence of the algorithm with iterations.

5.4.1. Influence of noise and number of sensors

In the above examples the noise is restricted to ± 1. The influence of increased proportion of noise is shown in Fig. 12. It is evident from the figure that with increase in noise there is reduction in accuracy of the algorithm.

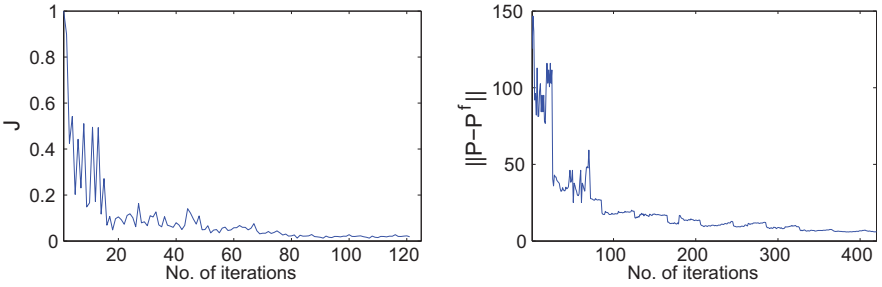

Fig. 11. (a) Convergence of the objective function J over the number of iterations and (b) convergence of l^2 error norm in parameter space over the number of iterations. The approximated level set values are denoted with P and with P^f the level set values corresponding to true void configuration.

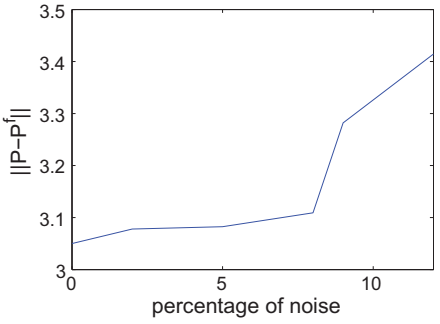

Fig. 12. The influence of noise on accuracy of the algorithm.

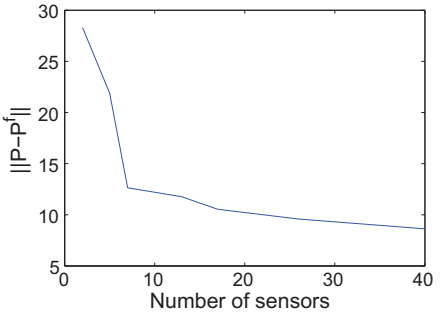

Fig. 13. The influence of number of sensors on accuracy of the algorithm.

On the other hand, the accuracy of the algorithm also depends on number of sensors along the measurement boundary. In order to study the influence of number of sensors on performance of the algorithm, an example problem of detecting a circular void of radius 0.75 cm located at the center of a square piezoelectric plate (10 cm $\times$ 10 cm) is solved several times, with different number of sensors each time. The error in parameter space with increasing number of sensors along the measurement boundary is shown in Fig. 13. The curve becomes almost asymptotic as the number of sensors exceeds seven. As mentioned earlier, the number of sensors used in all the numerical examples is 25 and these many sensors were sufficient to detect flaws located anywhere in the domain.

6. Conclusion

In this paper a methodology to detect multiple crack and void locations in a piezoelectric specimen is proposed. In each iteration, XFEM is used to solve the direct problem. The mesh remains unchanged in all iterations thereby considerably reducing computational time. The shape derivative and level sets are used to minimize the objective function. An adjoint problem is solved in each iteration to determine the shape derivative. Multiple setups are used to overcome the problem of local optima. The void configuration does not require external parameterization as it is implicitly represented by level sets. The numerical examples demonstrate the efficiency of the method in detecting any number of cracks and voids in specimen. The method proposed is more robust compared to iterative methods previously proposed in literature in which Genetic or search algorithms are used for the optimization. The method requires uniformly distributed voids all over the domain as initial configuration and so the method is not completely independent of initialization. In the future, the methodology will be extended to 3D and the response of piezoelectric specimen under dynamic loads may be utilized to construct the objective function.

References

[1] Z. Suo, C.M. Kuo, D.M. Barnett, J.R. Willis, Fracture mechanics for piezoelectric ceramics, J. Mech. Phys. Solids 40 (4) (1992) 739–765.
[2] Y.E. Pak, Linear electro-elastic fracture mechanics of piezoelectric materials, Int. J. Fract. 54 (1992) 79–100.
[3] H. Sosa, Plane problems in piezoelectric media with defects, Int. J. Solids Struct. 28 (4) (1991) 491–505.
[4] X.L. Xu, R.K.N.D. Rajapakse, Analytical solution for an arbitrarily oriented void/crack and fracture of piezoceramics, Acta Mater. 47 (6) (1999) 1735–1747.
[5] M. Kuna, Fracture mechanics of piezoelectric materials? Where are we right now?, Eng Fract. Mech. 77 (2010) 3635–3647.
[6] Y. Cai, X. Zhuang, H. Zhu, A generalized and efficient method for finite cover generation in the numerical manifold method, Int. J. Comput. Methods 10 (5) (2013) 1350028.
[7] Y. Cai, H. Zhu, X. Zhuang, A continuous/discontinuous deformation analysis (CDDA) method based on deformable blocks for fracture modeling, Front. Struct. Civ. Eng. 7 (2013) 369–378.
[8] M. Kuna, Finite element analyses of cracks in piezoelectric structures - a survey, Comput. Aided Des. 76 (2006) 725–745.
[9] G. Rus, R. Palma, J.L. Prez-Aparicio, Optimal measurement setup for damage detection in piezoelectric plates, Int. J. Eng. Sci. 47 (2009) 554–572.
[10] T. Lahmer, M. Kaltenbacher, B. Kaltenbacher, R. Lerch, FEM-based determination of real and complex elastic, dielectric and piezoelectric moduli in piezoceramic materials, IEEE Trans. Ultrason. Ferroelectr. Freq. Control 55 (2) (2008) 465–475.
[11] V.P. Nguyen, T. Rabczuk, S. Bordas, M. Duflot, Review: meshless methods: a review and computer implementation aspects, Math. Comput. Simul. 79 (3) (2008) 763–813.
[12] T. Rabczuk, G. Zi, A meshfree method based on the local partition of unity for cohesive cracks, Comput. Mech. 39 (6) (2007) 743–760.
[13] X. Zhuang, Y. Cai, C. Augarde, A meshless sub-region radial point interpolation method for accurate calculation of crack tip elds, Theor. Appl. Fract. Mec. 69 (2014) 118–125.
[14] X. Zhuang, H. Zhu, C. Augarde, An improved meshless Shepard and least square method possessing the delta property and requiring no singular weight function, Comput. Mech. 53 (2014) 343–357.
[15] X. Zhuang, C. Augarde, K. Mathisen, Fracture modeling using meshless methods and level sets in 3D: framework and modeling, Int. J. Numer. Meth. Eng. 92 (2012) 969–998.
[16] H. Zhu, X. Zhuang, Y. Cai, High rock slope stability analysis using the enriched meshless Shepard and least squares method, Int. J. Comput. Methods 8 (2011) 209–228.
[17] X. Liu, Y. Deng, Z. Zeng, L. Udpa, S.S. Udpa, Model-based inversion technique using element-free Galerkin method and state space search, IEEE Trans. Magn. 45 (3) (2009) 1486–1489.

[18] H. Waisman, E. Chatzi, A.W. Smyth, Detection and quantification of flaws in structures by the extended finite element method and genetic algorithms, Int. J. Numer. Methods Eng. 82 (2010) 303–328.
[19] D. Rabinovich, D. Givoli, S. Vigdergauz, XFEM-based crack detection scheme using a genetic algorithm, Comput. Fluids 71 (2007) 1051–1080.
[20] N. Moes, J. Dolbow, T. Belytschko, A finite element method for crack growth without remeshing, Int. J. Numer. Methods Eng. 46 (1) (1999) 133–150.
[21] P.M.A. Areias, T. Belytschko, Analysis of three-dimensional crack initiation and propagation using the extended finite element method, Int. J. Numer. Methods Eng. 63 (5) (2005) 760–788.
[22] J.M. Melenk, I. Babuska, The partition of unity finite element method: basic theory and applications, Comput. Methods Appl. Mech. Eng. 139 (1–4) (1996) 289–314.
[23] M. Stolarska, D.L. Chopp, N. Moes, T. Belytschko, Modeling crack growth by level sets in the extended finite element method, Int. J. Numer. Methods Eng. 51 (2001) 943–960.
[24] N. Sukumar, D.L. Chopp, N. Moes, T. Belytschko, Modeling holes and inclusions by level sets in the extended finite element method, Comput. Methods Appl. Mech. Eng. 190 (2001) 6183–6200.
[25] E. Chahine, P. Laborde, J. Pommier, Y. Renard, M. Salan, Study of some optimal XFEM type methods, Computational Methods in Applied Sciences, vol. 5, Springer, Netherlands, 2007.
[26] E. Bechet, M. Scherzer, M. Kuna, Application of the X-FEM to the fracture of piezoelectric materials, Int. J. Numer. Methods Eng. 77 (2009) 1535–1565.
[27] H.N. Vinh, I. Bakar, M.A. Msekh, J.H. Song, J. Muthu, G. Zi, P. Le, S. Bordas, R. Simpson, S. Natararajan, T. Lahmer, T. Rabczuk, Extended finite element method for dynamic fracture of piezo-electric materials, Eng. Fract. Mech. 92 (2012) 19–31.
[28] S.S. Nanthakumar, T. Lahmer, T. Rabczuk, Detection of flaws in piezoelectric structures using extended FEM, Int. J. Numer. Methods Eng. 96 (2013) 373–389.
[29] W. Huyer, A. Neumaier, Global optimization by multilevel coordinate search, J. Global Optim. 14 (1999) 331–355.
[30] G. Allaire, F. Jouve, A.M. Toader, Structural optimization using sensitivity analysis and a level-set method, J. Comput. Phys. 194 (2004) 363–393.
[31] P. Wei, M.Y. Wang, Structural optimization using sensitivity analysis and a level-set method, in: Proceedings of the TMCE, 2008.
[32] E. Bechet, H. Minnebol, N. Moes, B. Burgardt, Improved implementation and robustness study of the X-FEM for stress analysis around cracks, Int. J. Numer. Methods Eng. 64 (2005) 1033–1056.
[33] S. Osher, J.A. Sethian, Front propagating with curvature dependent speed: algorithms based on Hamilton–Jacobi formulations, J. Comput. Phys. 78 (1988) 12–49.
[34] H. Qi, D. Fang, Z. Yao, FEM analysis of electro-mechanical coupling effect of piezoelectric materials, Computat. Mater. Sci. 8 (1997) 283–290.
[35] B. Kaltenbacher, T. Lahmer, M. Mohr, M. Kaltenbacher, PDE based determination of piezoelectric material tensors, Eur. J. Appl. Math. 17 (2006) 383–416.
[36] T. Hao, Z. Shen, A new electric boundary condition of electric fracture mechanics and its applications, Eng. Fract. Mech. 47 (1994) 793–802.